UCLA
UCLA Previously Published Works

Title

Tetraanionic Biphenyl Lanthanide Complexes as Single-Molecule Magnets

Permalink

https://escholarship.org/uc/item/1t1354wf

Journal

Inorganic Chemistry, 54(5)

ISSN

0020-1669

Authors

Huang, Wenliang
Le Roy, Jennifer J
Khan, Saeed I
et al.

Publication Date

2015-03-02

DOI

10.1021/ic5029788

Copyright Information

Peer reviewed

Tetraanionic Biphenyl Lanthanide Complexes as Single-Molecule Magnets

Wenliang Huang,[†‖&] Jennifer J. Le Roy,[‡&] Saeed I. Khan,[†] Liviu Ungur,[§*] Muralee Murugesu,[‡*] and Paula L. Diaconescu[†*]

† Department of Chemistry and Biochemistry, University of California, Los Angeles, California 90095, USA

‡ Department of Chemistry, University of Ottawa, Ottawa, Ontario KIN 6N5, Canada

§ Theory of Nanomaterials Group and INPAC Institute for Nanoscale Physics and Chemistry, Katholieke Universiteit Leuven, Celestijnenlaan, 200F, 3001, Belgium

ABSTRACT: Inverse sandwich biphenyl complexes $[(NNTBS)Ln]_2(\mu\text{-biphenyl})[K(solvent)]_2$ ($NN^{TBS} = 1,1'\text{-fc}(NSi^tBuMe_2)_2$; Ln = Gd, Dy, Er; solvent = Et_2O, toluene; 18-crown-6), containing a quadruply reduced biphenyl ligand, were synthesized and their magnetic properties measured. One of the dysprosium biphenyl complexes was found to exhibit antiferromagnetic coupling and single-molecule magnet behavior with U_{eff} of 34 K under zero applied field. The solvent coordinated to potassium affected drastically the nature of the magnetic interaction, with the other dysprosium complex showing ferromagnetic coupling. Ab initio calculations were performed to understand the nature of magnetic coupling between the two lanthanide ions bridged by the anionic arene ligand and the origin of single molecule magnet behavior.

INTRODUCTION

Lanthanide single-molecule magnets (SMMs) show a fast improvement on increasing the anisotropic barrier and/or raising the blocking temperature limit to exhibit magnetic hysteresis.[1-3] Due to the complexity of the 4f shell, it is difficult to elucidate the electronic structure of paramagnetic lanthanide complexes, especially of those usually employed in SMMs, i.e. dysprosium and terbium.[4] Several methods have been proposed for predicting the anisotropic barriers of various lanthanide compounds with an emphasis on either a high or on a low symmetry coordination environment.[4-5] Despite these efforts, the factors governing a large magnetic anisotropy are beyond simple models, especially in molecules containing more than one 4f ion. A noticeable case is $[[((Me_3Si)_2N]_2(THF)Tb)_2(\mu\text{-}N_2)]^-$,[6] which exhibits magnetic hysteresis at a relatively high temperature (14 K) compared to other examples.[1-3] The strong exchange coupling induced by the bridging N_2^{3-} radical trianion was proposed to be responsible for the magnetic properties of this complex.[7] It is interesting to note that for actinides, an arene-bridged diuranium complex has shown SMM behavior.[8] However, structurally analogous arene-bridged lanthanide complexes have not been available until recently and, therefore, their magnetic properties could not be studied. Our group reported the synthesis of inverse sandwiches of biphenyl, $[(NN^{TBS})Ln]_2(\mu\text{-biphenyl})[K(solvent)]_2$ ($NN^{TBS} = 1,1'\text{-fc}(NSi^tBuMe_2)_2$; Ln = Sc, Y, La, Lu; solvent = Et_2O, toluene, THF, 18-crown-6),[9] containing a quadruply reduced biphenyl ligand and the metal ions coordinated to the same phenyl ring.

Experimental and computational studies indicated that the quadruply reduced biphenyl in $[(NN^{TBS})Ln]_2(\mu\text{-biphenyl})[K(solvent)]_2$ has the charge localized on the phenyl ring coordinated to the two rare earths. The overall molecule is stabilized by δ symmetry overlap between two π^* orbitals of the phenyl ring and metal-based orbitals. This similar electronic structure to diuranium arene complexes[8, 10-18] prompted us to explore the properties of the corresponding paramagnetic lanthanides, $[(NN^{TBS})Ln]_2(\mu\text{-biphenyl})[K(solvent)]_2$ (**Ln₂-biph**, Ln = Dy, Gd, and Er). More specifically, we focused our attention toward the highly anisotropic Kramer's ions dysprosium and erbium and the isotropic gadolinium analogue. The gadolinium compound provided an avenue to probe the nature and strength of the interaction between the metal centers. Herein, we report the synthesis and characterization of dysprosium, gadolinium, and erbium biphenyl complexes and a study of the magnetic properties of those complexes.

EXPERIMENTAL SECTION

General considerations. All experiments were performed under a dry nitrogen atmosphere using standard Schlenk techniques or an MBraun inert-gas glove box unless otherwise specified. Solvents, toluene, hexanes, diethyl ether (Et_2O), and tetrahydrofuran (THF) were purified using a two-column solid-state purification system by the method of Grubbs[19] and transferred to the glove box without exposure to air. *n*-Pentane was distilled over

calcium hydride under a dinitrogen atmosphere. Methanol was distilled over calcium oxide under a dinitrogen atmosphere. All solvents were stored on activated molecular sieves and/or sodium for at least a day prior to use. NMR solvents, benzene-d_6 (C_6D_6) and THF-d_8 (C_4D_8O) were obtained from Cambridge Isotope Laboratories, degassed or brought directly into a glove box in a sealed ampoule, and stored over activated molecular sieves for one week prior to use. Biphenyl was purchased from Sigma-Aldrich and used as received. 18-crown-6 was purchased from Alfa-Aesar and crystallized from hexanes after passing through an alumina plug. Benzyl potassium (KBn),[20] $H_2(NN^{TBS})$ (NN^{TBS} = 1,1′-fc(NSi^{t}BuMe$_2$)$_2$),[21] (NN^{TBS})GdI(THF)$_2$ and (NN^{TBS})ErI(THF)$_2$[22] were prepared following literature protocols. Nuclear magnetic resonance (NMR) spectra were recorded on Bruker AV300, Bruker DRX500, Bruker AV500 (work supported by the NSF grants CHE-1048804), or Bruker AV600 spectrometers at 25 °C in C_6D_6 or C_4D_8O unless otherwise specified. Chemical shifts are reported with respect to internal solvent (C_6D_6 at 7.16 ppm or C_4D_8O at 1.73 ppm). CHN analyses were performed in house on a CE-440 Elemental Analyzer manufactured by Exeter Analytical, INC.

Magnetic measurements. Magnetic susceptibility measurements for all complexes were obtained using a Quantum Design SQUID magnetometer MPMS-XL7 operating between 1.8 and 300 K for dc applied fields ranging from -7 to 7 T. Dc analyses were performed on polycrystalline samples sealed in a polyethylene membrane (prepared in an inert atmosphere) under a field ranging from 0 to 7 T and temperatures between 1.8 and 300 K. Ac susceptibility measurements were carried out under an oscillating ac field of 3 Oe and ac frequencies ranging from 1 to 1500 Hz. Magnetization data was collected at 100 K to check for ferromagnetic impurities that were absent in all samples. In addition, data were collected on different batches to check for consistency. Diamagnetic corrections were applied for the sample holder and the core diamagnetism from the sample (estimated with Pascal constants).

Ab initio calculations. All calculations on individual magnetic centers were done with MOLCAS 7.8 and are of CASSCF/RASSI/SINGLE_ANISO type. For Dy^{3+}: Active space of the CASSCF included 9 electrons in seven 4f orbitals. The spin-orbit coupling included the mixing of 21 sextets, 128 quartets and 130 doublet states. For Er^{3+}: Active space of the CASSCF included 11 electrons in seven 4f orbitals. The spin-orbit coupling included the mixing of 35 spin quartets, 112 spin doublet states. Two structures were employed: complete structure and reduced structure. In the reduced structure, all methyl and t-butyl groups were replaced by H. Three basis sets were employed (MB (minimal), DZP (medium) and TZP (large).

Synthesis of DyBr$_3$(THF)$_{3.5}$. DyBr$_3$(THF)$_{3.5}$ was synthesized following a protocol similar to that for GdBr$_3$(THF)$_{3.5}$.[22] In a 1 L three-neck round bottom flask, Dy$_2$O$_3$ (9.325 g, 25 mmol) and NH$_4$Br (20.060 g, 205 mmol) were added, followed by the addition of 120 mL of concentrated hydrobromic acid (48%, w/w aq.). The mixture was heated under a constant air flow to remove H$_2$O and HBr (which is absorbed by a 10% sodium hydroxide solution). After ca. 12 h, the resulted white solid

was transferred into a sublimation tube. The solid was heated under vacuum to remove water (140 °C for a minimum 8 h), to form (NH$_4$)$_3$(DyBr$_6$) (250 °C for 8 h), and eventually to dehydrate DyBr$_3$.[23] After cooling down to room temperature, the sublimation tube was brought into a glove-box and the fluffy off-white solid of DyBr$_3$ was separated from the rock-like NH$_4$Br crystals (which were located on the upper part of the tube). Yield for DyBr$_3$: 15.984 g, 79.5%. Solid DyBr$_3$ was then transferred into a 350 mL Schlenk tube and 50 mL of THF was carefully added (the reaction is highly exothermic and may result in boiling and even decomposition of THF to form carbon black). The white suspension was heated at 50 °C for 2 h. The volatiles were removed under reduced pressure to give a off-white microcrystalline solid. Yield for DyBr$_3$(THF)$_{3.5}$: 25.219 g, 96.9%. Overall yield from Dy$_2$O$_3$: 77.0%. The empirical formula DyBr$_3$(THF)$_{3.5}$ was determined by considering the mass change upon treatment with THF[22] and was used as such in subsequent procedures.

Synthesis of (NN^{TBS})DyI(THF)$_2$. (NN^{TBS})DyI(THF)$_2$ was synthesized following a protocol similar to that for (NN^{TBS})GdI(THF)$_2$.[22] In a 100 mL round bottom flask were added DyBr$_3$(THF)$_{3.5}$ (1.0000 g, 1.528 mmol) and 60 mL of THF. The suspension was chilled with a dry ice / acetone bath for 15 min. In a 20 mL scintillation vial were added KBn (0.5970 g, 4.584 mmol) and 15 mL of THF to give a red solution, which was chilled with a dry ice / acetone bath for 10 min. The KBn solution was added dropwise to the DyBr$_3$ suspension with stirring and constant chilling by the dry ice / acetone bath. Shortly after the addition, the red color of KBn disappeared and the resulting grey suspension was allowed to stir at 0 °C (ice bath) for 30 min. The suspension was then filtered through Celite and washed with ca. 10 mL of THF. The washings were combined with the filtrate and transferred into a clean 100 mL round bottom flask (ca. 70 mL). The grey solution (*in situ* formed DyBn$_3$(THF)$_3$) was chilled with a dry ice / acetone bath for 15 min. In a 20 mL scintillation vial were added H$_2$(NN^{TBS}) (0.6790 g, 1.527 mmol) and 10 mL of THF. The vial was chilled with a dry ice / acetone bath for 10 min. H$_2$(NN^{TBS}) solution was added dropwise to the DyBn$_3$(THF)$_3$ solution with stirring and constant chilling with a dry ice / acetone bath. After addition, the solution color turned to orange. The solution was stirred at 0 °C (ice bath) for 1 h before removing the volatiles. After removing volatiles, the resulted orange solid was extracted into ca. 20 mL of toluene and filtered through Celite to remove any remaining insoluble impurities. To the orange solution (*in situ* formed (NN^{TBS})DyBn(THF)) was added 2 mL of a toluene solution of Me$_3$SiI (0.6110 g, 3.054 mmol) at 25 °C. The solution was allowed to stir at 25 °C for 1 h. Then ca. 2 mL of THF was added to quench the excess Me$_3$SiI and the volatiles were removed under reduced pressure to yield an orange solid. Crystallization from a minimum amount of Et$_2$O (ca. 20 mL) layered with *n*-pentane (ca. 20 mL) at -35 °C yielded orange crystals of (NN^{TBS})DyI(THF)$_2$. Yield: 1st crop 0.7104 g, 52.7%. The mother liquor was concentrated to yield a 2nd crop of 0.205 g, 15.5%. Total yield: 68.2%. Single crystals of (NN^{TBS})DyI(THF)$_2$ were grown from an Et$_2$O solution layered with *n*-pentane. Anal. (%): Calcd. for C$_{30}$H$_{54}$N$_2$O$_2$FeDySi$_2$I with one molecule of *n*-pentane

(C_5H_{12}), M_w = 948.346: C, 44.32; H, 7.02; N, 2.95. Found: C, 44.26; H, 6.94; N, 2.96.

Synthesis of Dy$_2$-biph. **Dy$_2$-biph** was synthesized following a protocol similar to that for **Y$_2$-biph**.[9] In a 20 mL scintillation vial, (NN^{TBS})DyI(THF)$_2$ (0.4000 g, 0.457 mmol) and biphenyl (0.0352 g, 0.228 mmol) were dissolved in ca. 10 mL of THF. The vial was chilled with a dry ice / acetone bath for 10 min. KC$_8$ (0.1543 g, 1.141 mmol) was added to the THF solution. The mixture was warmed up to 25 °C and allowed to stir for 10 min before filtering through Celite to remove the byproducts, graphite and potassium iodide. The volatiles were removed under reduced pressure to yield a black solid. The solid was washed with ca. 15 mL of Et$_2$O and a microcrystalline black solid of **Dy$_2$-biph** was collected on a medium frit. Yield: 0.2550 g, 70.2%. **Dy$_2$-biph** synthesized as such has a formula of [(NN^{TBS})Dy]$_2$(m-biphenyl)[K(OEt$_2$)]$_2$. Single crystals of **Dy$_2$-biph** were grown from a toluene solution layered with hexanes with a formula of [(NN^{TBS})Dy]$_2$(m-biphenyl)[K(toluene)]$_2$. Anal. (%): Calcd. for $C_{64}H_{106}N_4O_2Fe_2Dy_2Si_4K_2$ (with one Et$_2$O as a coordinating solvent for each potassium), M_w = 1590.808: C, 48.32; H, 6.72; N, 3.52. Found: C, 48.06; H, 6.76; N, 3.85.

Synthesis of Dy$_2$-biph-crown$_2$. **Dy$_2$-biph** (0.0949 g, 0.0597 mmol) and 2 equiv 18-crown-6 (0.0315 g, 0.119 mmol) were weighed in a 20 mL scintillation vial. Cold THF (5 mL) was added and the mixture was allowed to stir at -78 °C for 1 h. Volatiles were removed under reduced pressure and the resulting solid was washed with Et$_2$O. The black solid was then dissolved in THF and the solution layered with *n*-pentane. Black crystals formed after storing the solution in a -35 °C freezer for 1 d. Yield: 0.1182 g, 93.5%. Single crystals of **Dy$_2$-biph-crown$_2$** were grown from a THF solution layered with *n*-pentane. Anal. (%): Calcd. for $C_{88}H_{150}N_4O_{14}Fe_2Dy_2Si_4K_2$ (with one THF molecule coordinated to potassium in addition to 18-crown-6), M_w = 2115.414: C, 49.97; H, 7.15; N, 2.65. Found: C, 49.33; H, 6.98; N, 2.70.

Synthesis of Gd$_2$-biph. **Gd$_2$-biph** was synthesized following a protocol similar to that for **Dy$_2$-biph**. Scale: (NN^{TBS})GdI(THF)$_2$ (0.3000 g, 0.344 mmol), biphenyl (0.0266 g, 0.172 mmol), and KC$_8$ (0.1164 g, 0.861 mmol). Yield: 0.1950 g, 71.6%. **Gd$_2$-biph** synthesized as such has a formula of [(NN^{TBS})Gd]$_2$(m-biphenyl)[K(OEt$_2$)]$_2$. Single crystals of **Dy$_2$-biph** were grown from a toluene solution layered with hexanes with a formula of [(NN^{TBS})Gd]$_2$(m-biphenyl)[K(toluene)]$_2$. Anal. (%): Calcd. for $C_{64}H_{106}N_4O_2Fe_2Gd_2Si_4K_2$ (with one Et$_2$O as a coordinating solvent for potassium), M_w = 1580.308: C, 48.64; H, 6.76; N, 3.54. Found: C, 48.38; H, 6.63; N, 3.47.

Synthesis of Gd$_2$-biph-crown$_2$. **Gd$_2$-biph** (0.1345 g, 0.0851 mmol) and 2 equiv 18-crown-6 (0.0440 g, 0.166 mmol) were weighed in a scintillation vial. Cold THF (5 mL) was added and the mixture was allowed to stir at -78 °C for 1 h. Volatiles were removed under reduced pressure and the resulting solid was washed with Et$_2$O. The black solid was then dissolved in THF and the solution layered with *n*-pentane. Black crystals formed after storing the solution in a -35 °C freezer for 1 d. Yield: 0.1200 g, 67.0%. Single crystals of **Dy$_2$-biph-crown$_2$** were grown from a THF solution layered with *n*-pentane. Anal. (%): Calcd. for $C_{88}H_{150}N_4O_{14}Fe_2Gd_2Si_4K_2$ (with one THF molecule

coordinated to potassium in addition to 18-crown-6), M_w = 2104.914: C, 50.23; H, 7.19; N, 2.66. Found: C, 50.31; H, 7.27; N, 2.78.

Synthesis of Er$_2$-biph. **Er$_2$-biph** was synthesized following a protocol similar to that for **Dy$_2$-biph**. Scale: (NN^{TBS})ErI(THF)$_2$ (0.4000 g, 0.454 mmol), biphenyl (0.0350 g, 0.227 mmol), and KC$_8$ (0.1535 g, 1.135 mmol). Yield: 0.2413 g, 66.4%. **Er$_2$-biph** synthesized as such has a formula of [(NN^{TBS})Er]$_2$(μ-biphenyl)[K(OEt$_2$)]$_2$. Single crystals of **Er$_2$-biph** were grown from an Et$_2$O solution. Anal. (%): Calcd. for $C_{64}H_{106}N_4O_2Fe_2Er_2Si_4K_2$ (with one Et$_2$O as a coordinating solvent for potassium) and one extra Et$_2$O molecule, M_w = 1674.451: C, 48.77; H, 6.98; N, 3.35. Found: C, 49.49; H, 6.28; N, 3.50.

Synthesis of Er$_2$-biph-crown$_2$. **Er$_2$-biph** (0.1045 g, 0.0653 mmol) and 2 equiv 18-crown-6 (0.0345 g, 0.131 mmol) were weighed in a 20 mL scinillation vial. Cold THF (5 mL) was added and the mixture was allowed to stir at -78 °C for 1 h. Volatiles were removed under reduced pressure and the resulting solid was washed with Et$_2$O. The black solid was then dissolved in THF and the solution layered with *n*-pentane. Black crystals formed after storing the solution in a -35 °C freezer for 1 d. Yield: 0.1307 g, 95.2%. Single crystals of **Er$_2$-biph-crown$_2$** were grown from a THF solution layered with *n*-pentane. Anal. (%): Calcd. for $C_{88}H_{150}N_4O_{14}Fe_2Er_2Si_4K_2$ (with one THF molecule coordinated to potassium in addition to 18-crown-6) and 1.5 molecules of hexanes (C_6H_{14}), M_w = 2326.306: C, 52.15; H, 7.76; N, 2.41. Found: C, 52.60; H, 7.13; N, 2.55.

RESULTS AND DISCUSSION

Synthesis and Characterization of Tetraanionic Biphenyl Lanthanide Complexes. The metal precursors (NN^{TBS})LnI(THF)$_2$ (**LnI**, Ln = Dy, Gd, and Er) can be synthesized following a similar protocol to that developed for other paramagnetic lanthanides.[22] Compounds **Gd$_2$-biph**, **Dy$_2$-biph**, and **Er$_2$-biph** could be isolated in high yield analogously to **Y$_2$-biph** (Scheme 1a).[9] Similar to **Y$_2$-biph**, the separated ion pair version, ([(NN^{TBS})Ln]$_2$(μ-biphenyl))[K(18-crown-6)(THF)$_{1.5}$]$_2$ (**Ln$_2$-biph-crown$_2$**, Ln = Dy, Gd, and Er), could also be synthesized by treating **Ln$_2$-biph** with two equivalents of 18-crown-6 followed by crystallization from THF/*n*-pentane. (Scheme 1b).

Scheme 1. (a) Synthesis of **Ln$_2$-biph**; (b) **Ln$_2$-biph-crown$_2$** (Ln = Gd, Dy, and Er).

The molecular structures of **Ln₂-biph** and **Ln₂-biph-crown₂** (Ln = Dy, Gd, and Er) were determined by X-ray crystallography; those of **Dy₂-biph** and **Dy₂-biph-crown₂** are shown in Figure 1 as representative examples. Crystallized from a toluene solution layered with hexanes, **Dy₂-biph** and **Gd₂-biph** are isostructural to **Y₂-biph** with a toluene molecule as the coordinating solvent for K^+. However, **Er₂-biph**, which is crystallized from a diethyl ether solution, has diethyl ether as a coordinating solvent for K^+. Despite the difference in the coordinating solvent for K^+, the coordination environment around each lanthanide ion is similar in all **Ln₂-biph**.

Table 1 summarizes some informative structural parameters for **Ln₂-biph** and **Ln₂-biph-crown₂**. The average Ln-N, Ln-C, and Ln-Ln distances follow the general trend of the ionic radii of metal ions. The Ln-Ln distances are rather short at 4.268(1), 4.194(1), and 4.138(1) Å for Gd, Dy, and Er, respectively, for **Ln₂-biph**. The Dy-Dy distance is comparable to the Dy-Dy distance of 4.14 Å in the triple decker complex Dy₂(COT″)₃ (COT″ = 1,4-bis(trimethylsilyl)cyclooctatetraenyl dianion).[24]
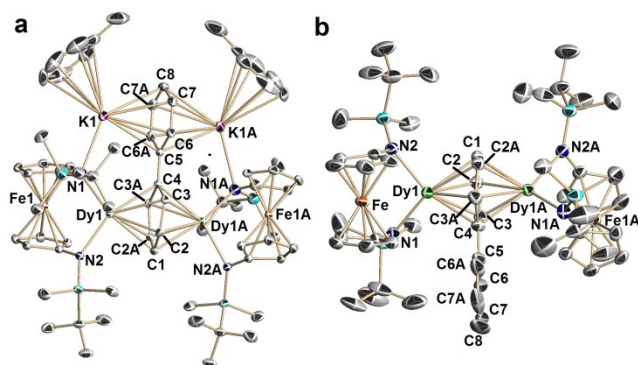
Figure 1. Molecular structures of (a) **Dy₂-biph-toluene** and (b) **Dy₂-biph-crown₂** with thermal ellipsoids drawn at the 50% probability level. Hydrogen atoms and disordered counterparts were omitted for clarity.

The Ln-C and Ln-Ln distances are even shorter in the separated ion pair complexes **Ln₂-biph-crown₂**. For example, the average Dy-C distance and Dy-Dy distance in **Dy₂-biph-crown₂** is 2.525(7) and 4.107(2) Å, respectively, 0.03 and 0.08 Å shorter than the corresponding parameters of **Dy₂-biph**. Together with the longer average C-C distance found for the phenyl ring coordinated to the lanthanides, these structural features reflect a stronger metal arene interaction and a more localized charge on the coordinating phenyl ring upon exclusion of potassium.

In the previous **Ln₂-biph** series (Ln = Sc, Y, and Lu), we noticed the following trend in the torsion angle (defined by the dihedral angle C2-C3-C3A-C2A and C3-C2-C2A-C3A in Figure 1a and indicating the degree of distortion from planarity) of the coordinated phenyl ring: the smaller the metal ions, the larger the torsion angle. This trend is also observed for **Gd₂-biph**, **Dy₂-biph**, and **Er₂-biph**. In addition, the dihedral angle Fe-Ln-Ln-Fe (Fe1-Dy1-Dy1A-Fe1A in Figure 1a) is a measure of the relative position of the two lanthanide units. Upon the removal of K^+ by 18-crown-6, a significant decrease of that angle was observed for all lanthanides (Gd: 26°; Dy: 34°; Er: 19°).

Table 1. Structural parameters for **Ln₂-biph** (Ln1 in table, Ln = Gd / Dy / Er) and **Ln₂-biph-crown₂** (Ln2 in table, Ln = Gd / Dy / Er) (distances in Å and angles in °).

|	Gd1	Gd2	Dy1	Dy2	Er1	Er2
$R(Ln)^1$	1.08	1.08	1.05	1.05	1.03	1.03
Ln-Ln	4.27	4.22	4.19	4.11	4.14	4.07
Ln-Fe	3.20	3.25	3.21	3.26	3.23	3.26
Ln-N²	2.37	2.38	2.33	2.33	2.31	2.31
Ln-C²,³	2.58	2.57	2.55	2.53	2.53	2.51
C-C⁴	1.46	1.46	1.46	1.47	1.46	1.47
C_{ipso}-C_{ipso}	1.41	1.46	1.41	1.42	1.42	1.44
Torsion⁵	10	12	-11	-11	-14	-14
Dihedral⁶	-162	-136	161	127	145	126

[1]From ref;[25] [2]average value for Ln-N and Ln-C distances; [3]carbon atoms of coordinated phenyl ring; [4]average C-C distance in the coordinated phenyl ring; [5]torsion angle defined by the average of the dihedral angle C_{meta}-C_{ortho}-C_{ortho}-C_{meta} and C_{ortho}-C_{meta}-C_{meta}-C_{ortho} of the coordinated phenyl ring; [6]dihedral angle Fe-Ln-Ln-Fe.

Magnetism of Tetraanionic Biphenyl Lanthanide Complexes. Solid-state magnetic properties of all six complexes were investigated using a superconducting quantum interference device (SQUID). Analyses were performed on crushed polycrystalline samples sealed in a polyethylene membrane prepared and sealed under an inert atmosphere. Direct current (dc) susceptibility measurements were carried out under a 0.1 T applied dc field over the temperature range of 1.8-300 K (Figure 2). The room temperature χT values of 28.59 cm³Kmol⁻¹ (**Dy₂-biph**) and 27.95 cm³Kmol⁻¹ (**Dy₂-biph-crown₂**) are in good agreement with the theoretical value of 28.34 cm³Kmol⁻¹ for two non-interacting dysprosium(III) ions ($^6H_{15/2}$, $S = 5/2$, $L = 5$, $g_J = 4/3$). Similarly, the room temperature χT values of 21.87 cm³ K mol⁻¹ (**Er₂-biph**) and 22.59 cm³Kmol⁻¹ (**Er₂-biph-crown₂**) are in good agreement with the theoretical value of 22.96 cm³Kmol⁻¹ for two non-interacting erbium(III) ions ($^4I_{15/2}$, $S = 3/2$, $L = 6$, $g_J = 6/5$). Lastly, for **Gd₂-biph** and **Gd₂-biph-crown₂** the respective room temperature χT values of 15.63 cm³Kmol⁻¹ and 15.83 cm³ K mol⁻¹ are in good agreement with the theoretical value of 15.76 cm³ K mol⁻¹ for two non-interacting gadolinium(III) ions ($^8S_{7/2}$, $S = 7/2$, $L = 0$, $g_J = 2$).

The χT product of **Dy₂-biph** decreases gradually from 300 K with decreasing temperature with a steep decrease below 20 K to reach a minimum value of 18.73 cm³Kmol⁻¹ at 1.8 K. The low temperature decrease may be attributed to several factors including significant anisotropy inherent to dysprosium(III) ions as well as an anti-ferromagnetic interaction between dysprosium centers. The χT product of **Dy₂-biph-crown₂** shows similar behavior to **Dy₂-biph** from 300 to 20 K, however, interestingly, below 20 K there is a sharp increase to reach a maximum value of 29.19 cm³Kmol⁻¹ at 1.8 K, indicating the presence of dominant ferromagnetic interactions between the spin carriers. This

4

interaction is likely intramolecular in nature as the closest intermolecular dysprosium-dysprosium distance is 14.25 Å. This remarkable change in magnetic properties due to the secondary coordination environment is in agreement with recently reported results, showing that the overall properties of lanthanide SMMs can be altered by small structural modifications.[26]

The variable temperature χT plots of the two erbium complexes resemble the data for **Dy₂-biph-crown₂**. A slight decrease of the χT product was observed up to 20 K followed by a sharp increase reaching maximum values of 21.87 cm³Kmol⁻¹ for **Er₂-biph** and 30.06 cm³Kmol⁻¹ for **Er₂-biph-crown₂** at 1.8 K. Such behavior indicates again ferromagnetic interactions between the two erbium ions in both complexes. As the dysprosium and erbium systems are highly anisotropic, employment of Kambe's coupling method to obtain the coupling strength is not valid, thus we focused our efforts in attaining coupling strength in the isotropic gadolinium analogues. For **Gd₂-biph** and **Gd₂-biph-crown₂**, the χT product remains fairly linear with decreasing temperature, with a sharp decrease below 50 K to reach minimum values at 1.8 K of 1.17 cm³Kmol⁻¹ and 0.94 cm³Kmol⁻¹, respectively. In both **Gd₂-biph** and **Gd₂-biph-crown₂**, this low temperature decrease is primarily caused by antiferromagnetic coupling between isotropic gadolinium ions.
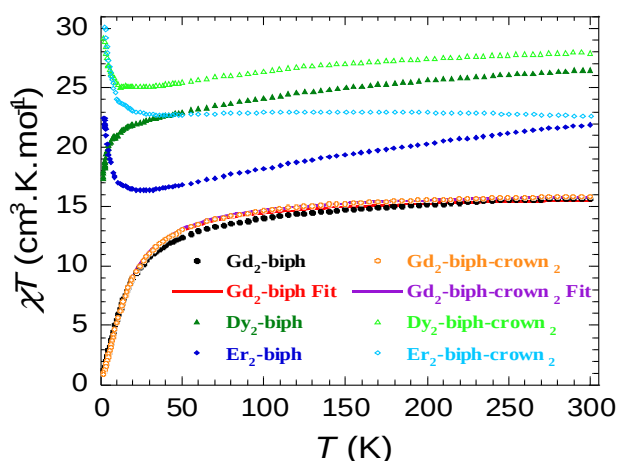
Figure 2. Temperature dependence of the χT product at 0.1 T for **Gd₂-biph** (●), **Gd₂-biph-crown₂** (O), **Dy₂-biph** (▲), **Dy₂-biph-crown₂** (Δ), **Er₂-biph** (♦), and **Er₂-biph-crown₂** (◊), with χ being the molar susceptibility per molecule defined as M/H.

In order to quantify the strength of the gadolinium–gadolinium interaction in both complexes, application of the Van Vleck equation to the Kambe's vector coupling method was employed using the isotropic spin Hamiltonian $H = -2J S_a \cdot S_b$ with $S_a = S_b = 7/2$, which was used to fit the variation of the χT versus T data. The best-fit parameters obtained are $J = -0.642(6)$ cm⁻¹, $g = 2.01(7)$ and $J = -0.664(6)$ cm⁻¹, $g = 2.03(7)$ for **Gd₂-biph** and **Gd₂-biph-crown₂**, respectively. Although relatively weak, the gadolinium–gadolinium coupling in both complexes surprisingly shows an increase in J over the COT-bridged Gd$^{III}_2$ complex[24] ($J = -0.447(7)$ cm⁻¹) despite a similar Ln-Ln

separation. This suggests that, in the present arene-bridged system, the Ln-C$_{biph}$ interaction is stronger than Ln-C$_{COT}$, which is likely a consequence of the significant metal-phenyl orbital overlap, as shown by DFT calculations on the diamagnetic counterpart, **Y₂-biph**.[9] The slight difference in J between **Gd₂-biph** and **Gd₂-biph-crown₂** is consistent with a decreasing gadolinium–gadolinium distance. A difference in magnetic coupling (ferromagnetic *vs.* antiferromagnetic) of different lanthanide analogues, such as that observed in **Dy₂-biph-crown₂**, **Er₂-biph-crown₂**, and **Gd₂-biph-crown₂**, has been previously reported by Ishikawa *et al.*[27] However, when considering all six complexes, it is interesting that ferromagnetic interactions are observed in complexes with closer Ln-Ln distances (4.14 Å or less) and antiferromagnetic interactions are observed in **Dy₂-biph**, **Gd₂-biph-crown₂** and **Gd₂-biph**, each having Ln-Ln distances greater than 4.14 Å.

In order to determine the presence of magnetic anisotropy, field-dependent magnetization measurements were performed on all six complexes between 1.8 and 7 K at fields ranging from 0 to 7 T (Figures S8-13). In **Dy₂-biph** and **Dy₂-biph-crown₂**, the magnetization data below 7 K revealed a rapid increase in the magnetization at low magnetic fields with a more gradual increase above 2 T reaching near-saturation at low temperatures ($M = 9.62(6)$ μB at 1.8 K under 7 T (**Dy₂-biph**); $M = 10.5(1)$ μB at 1.8 K under 7 T (**Dy₂-biph-crown₂**)). Both the non-saturation in the M *vs.* H data as well as the non-superimposition of isotemperature lines in the M *vs.* H/T plot suggests non-negligible magnetic anisotropy in both complexes (Figures S8, S9). Both **Er₂-biph** and **Er₂-biph-crown₂** exhibit near identical magnetization and reduced magnetization behavior with their respective dysprosium analogues hence magnetic anisotropy is also present in these complexes. Near-saturation at 1.8 K is observed in the magnetization data of **Er₂-biph**, with M = 7.77(4) μB, and **Er₂-biph-crown₂**, with M = 7.74(5) μB under 7 T. In contrast to the dysprosium and erbium complexes, the reduced magnetization measurements performed on **Gd₂-biph** and **Gd₂-biph-crown₂** reveal a linear relationship as expected for an antiferromagnetically coupled isotropic spin carriers. Due to the dominant antiferromagnetic coupling at low temperatures, the spin ground state for the gadolinium analogue is expected to be a singlet. Therefore the observed linear curves are likely due to the presence of low lying excited states which are thermally accessible. The isotropic nature of gadolinium precludes the possibility of SMM behavior in **Gd₂-biph** and **Gd₂-biph-crown₂** complexes.

In order to investigate the magnetic relaxation dynamics of the dysprosium and erbium complexes, alternating current (ac) magnetic susceptibility measurements were performed. For **Dy₂-biph**, under zero applied dc field, a strong temperature and frequency-dependent χ" signal was observed. Temperature-dependent χ" data revealed full frequency-dependent peaks with peak maxima shifting toward lower temperatures between 9-4.5 K, consistent with SMM behavior (Figure S14). Below 4.5 K, frequency independent peaks are observed indicating quantum tunneling of the magnetization (QTM) at low temperature.

5

Dy₂-biph due to shorter metal-metal distances; thus, by coupling ferromagnetically two Kramer's dysprosium ions, an integer spin is obtained as the spin ground state for **Dy₂-biph-crown₂**. This subsequently increases the QTM and disappearance of the SMM behavior.

Figure 3. Out-of phase (χ") ac magnetic susceptibility for **Dy₂-biph** (a) and **Dy₂-biph-crown₂** (b) from 1.8 – 9 K under an applied dc field of 900 Oe.

The anisotropic barrier, U_{eff} = 34 K, τ_0 = 1.6 × 10⁻⁶ s, was determined by using an Arrhenius equation ($\tau = \tau_0$ exp(U_{eff}/kT)). This barrier is relatively small compared to those of other didysprosium SMMs,[2] but is comparable to that for the aromatic COT" bridged complex, Dy₂(COT")₃ (COT" = 1,4-(SiMe₃)₂-COT, U_{eff} = 25 K, τ_0 = 1.6 × 10⁻⁶ s).[24] This relatively small barrier is attributed to the presence of significant QTM observed in the χ" data (Figure S14). Upon application of an optimum static dc field of 900 Oe, QTM was reduced in **Dy₂-biph** (Figure 3, S15). As expected, a decrease of the frequency independent peak maxima in the χ" data below 4.5 K (Figure 3) was observed as well as a significant improvement in the anisotropic barrier; U_{eff} = 53 K, τ_0 = 1.5 × 10⁻⁷ s (Figure S16). The antiferromagnetic dysprosium-dysprosium interaction (determined from the χT data) implies that this energy barrier originates from a single ion effect as observed in the previously reported Dy₂(COT")₃ (COT" = 1,4-(SiMe₃)₂-COT) complexes.[24]

The ac magnetic susceptibility of **Dy₂-biph-crown₂** was radically different from that of **Dy₂-biph**: surprisingly, no ac signal was observed under zero applied dc field. However, under a 900 Oe applied dc field frequency dependent studies reveal a peak at low frequency and an additional tail at high frequency at 1.8 K (Figures 3 and S17). The observed peak is frequency independent with varying temperature and, therefore, signifies a significant QTM relaxation process. Surprisingly, even under an applied dc field, no clear blocking of the magnetization was observed in **Dy₂-biph-crown₂**, therefore, no energy barrier could be extracted for this complex. As mentioned previously, it has been recently demonstrated that even small changes in the secondary coordination sphere can have a large impact on the magnetic anisotropy axis of lanthanide(III) ions.[24, 26] The decrease in magnetic performance of **Dy₂-biph-crown₂** compared to **Dy₂-biph** is unexpected due to the ferromagnetic interaction between dysprosium ions in **Dy₂-biph-crown₂** and antiferromagnetic interaction in **Dy₂-biph**. These results are additionally surprising when the smaller coordination environment around each dysprosium ion in **Dy₂-biph** compared to **Dy₂-biph-crown₂** is considered. A small coordination environment in such low symmetry complexes can quench the orbital angular momentum due to increased electron repulsion, therefore, the stronger magnetic performance of **Dy₂-biph** is again unexpected.[1] However, it is noteworthy that the dysprosium-dysprosium interactions in **Dy₂-biph-crown₂** are likely stronger than in

Figure 4. Out-of phase (χ") ac magnetic susceptibility for **Er₂-biph** (a) and **Er₂-biph-crown₂** (b) from 1.8 – 6 K under an applied dc field of 900 Oe.

In contrast, **Er₂-biph** and **Er₂-biph-crown₂** display similar ac magnetic relaxation dynamics. Under zero applied dc field, both complexes display a tail in the out-of phase (χ") susceptibility (Figures S18-19) at high frequency. Such behavior precludes zero field SMM behavior in these complexes. Under a 900 Oe applied dc field, both **Er₂-biph** and **Er₂-biph-crown₂** display multiple relaxation dynamics (Figures 4, S20-21). At high frequency, **Er₂-biph** displays full frequency-dependent peaks with peak maxima shifting towards lower temperatures indicating slow magnetic relaxation. A secondary peak is also evident at low temperatures and frequency, where peak maxima are frequency independent indicating QTM. Similarly, **Er₂-biph-crown₂** also displays full frequency-dependent peaks indicating a thermal relaxation process as well as a secondary shoulder at low frequency consistent with a secondary QTM relaxation process. In both **Er₂-biph** and **Er₂-biph-crown₂**, the anisotropic barrier was extracted from the frequency-dependent peaks yielding U_{eff} = 16 K, τ_0 = 3.4 × 10⁻⁵ s and U_{eff} = 25 K, τ_0 = 4.7 × 10⁻⁶ s respectively (Figures S22-23).

Ab initio Calculations. Ab initio calculations were employed in order to acquire more insight into the electronic and magnetic structure and the origin of the magnetic blocking of the investigated compounds. All calculations were performed with MOLCAS program package[28] and were of CASSCF/RASSI/SINGLE_ANISO type[29] (see the ESI for computational results and details). This computational approach has been successfully applied before for the investigation of lanthanide compounds.[30-32] In particular, this computational methodology proved reliable in determination of the orientation of the local magnetic axes in the lowest electronic states of metal sites,[33] and quite recently, it was proved to give also trustworthy spectrum of the crystal field splitting of the lowest J manifolds of lanthanide based complexes.[34]

Current ab initio calculations are not suitable for treating several magnetic centers at a time. Therefore suitable fragmentation was imposed. Fragmentation, in our approach, does not imply "deleting atoms from the molecular structure" but rather consists only in replacement of neighboring magnetic sites by their diamagnetic

6

equivalent. In the present case, Lu^{3+} was used in place of neighboring Dy^{3+} or Er^{3+} sites. All Fe^{II} sites were kept as they are in all calculations, due to their low–spin structure. In all cases, the experimental X-ray structure was used for all calculations without further optimization of the atom positions by computational means. All atoms were described by ANO-RCC relativistic basis sets[35] available in the MOLCAS package.[28] The active space of the CASSCF method included all electrons from the last shell spanning seven $4f$ orbitals. All spin states arising from this active space were optimized and all (for Er) or some (for Dy) of them were further mixed by spin-orbit interaction in the RASSI program. On the basis of the resulting spin-orbital multiplets, magnetic properties of individual Ln sites (i.e. main magnetic axes) were evaluated. Table 2 shows the obtained low-lying energy spectrum of individual Ln sites for all investigated compounds in the largest computational model employed. We noticed that the total crystal field splitting of the ground J=15/2 manifold for **Dy₂-biph** and **Dy₂-biph-crown₂** is almost twice as large as that of **Er₂-biph** and **Er₂-biph-crown₂**. This sharp difference is attributed to the different nature of the ground $J = 15/2$ manifold of Er^{3+} and Dy^{3+} ions, in particular reflected in different Stevens parameters α, β, and γ corresponding to the crystal-field operators O_2, O_4, and O_6.[36] The splitting between the ground and the first excited Kramers doublets is about 90 cm^{-1} for **Dy₂-biph** and about 51 cm^{-1} for **Dy₂-biph-crown₂**. We also noticed the much stronger magnetic axiality for the former compound, reflected in the $g_{X,Y}$ values: for the latter compound, they are nearly one order of magnitude larger than in the former one. Due to the lack of symmetry in **Er₂-biph**, Er sites are chemically and electronically different. This is reflected in the obtained energy spectrum of individual Er sites and in their magnetic axiality. Figure 5 shows the ab initio calculated main magnetic axes and orientation of the local magnetic moments in the ground state with respect to the molecular frame for **Dy₂-biph** and **Dy₂-biph-crown₂** Magnetic axes of **Er₂-biph** and **Er₂-biph-crown₂** are shown in the Supporting Information (Figures S24 and S25).
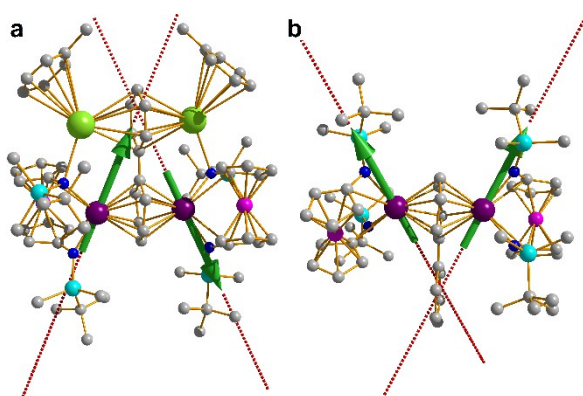
Figure 5. Ab initio calculated main magnetic axes (dashed lines) and orientation of the local magnetic moments in the ground state for **Dy₂-biph** (a) and **Dy₂-biph-crown₂** (b) with respect to the molecular frame. Color scheme: Dy-purple; Fe-pink; K-light green; Si-cyan; C-grey; N-blue. H atoms are not shown for clarity.

We note that the magnetic axiality is higher for the Er site, which has a larger energy gap between the ground and first excited Kramers doublets. For **Er₂-biph-crown₂**, ab initio calculations revealed a relatively small energy gap between ground and first excited doublets and a relatively low magnetic axiality. Interestingly, the main anisotropy axis of both **Dy₂-biph** and **Dy₂-biph-crown₂** makes a small angle with the shortest chemical bond of the corresponding Dy site, while the main anisotropy axes of **Er₂-biph** and **Er₂-biph-crown₂** are almost perpendicular to the shortest Er-N chemical bond. This is due to the opposite signs of the Stevens parameters α and β for the ground $J = 15/2$ of Dy^{3+} and Er^{3+} ions: for the same crystal field parameters, the splitting effect arising from second- and fourth-rank parameters is opposite.[36] For the investigated compounds, the nitrogen atoms hold a relatively large electrostatic charge (computed Mulliken charges vary from -0.55 to -0.70), which, corroborated with the short distance, induces strong electrostatic and covalent effects, resulting in the largest perturbation to the corresponding Ln site. Since this perturbation induces the orientation of the main magnetic axis for the ground doublet along the Dy-N chemical bond for Dy sites, the magnetic axis of the Kramers doublet that is "destabilized" the most, i.e., the 8ᵗʰ doublet in Table 2, is lying almost perpendicularly to the shortest Dy-N chemical bond. Consequently, due to the opposite signs of the Stevens parameters α and β for the ground manifold $J = 15/2$ of Dy^{3+} and Er^{3+}, for Er compounds, this perturbation will stabilize the ground Kramers doublet holding the perpendicular orientation of the main magnetic axis to the shortest chemical bond (Table 2). A similar, opposite effect of the almost identical crystal field on the magnetic anisotropy of Er and Dy ions was recently found for $[Er(COT)_2]^-$ SIM.[30]

Table 2. Energies of the low-lying doublet states arising from the splitting of the ground $J = 15/2$ of individual Ln sites in the investigated compounds (cm^{-1}).

	Dy₂-biph	Dy₂-biph-crown₂	Er₂-biph		Er₂-biph-crown₂
			Er1	Er2	
1	0.0	0.0	0.0	0.0	0.0
2	90.4	50.8	57.9	87.3	22.0
3	233.4	191.1	158.7	174.2	163.7
4	383.4	330.0	194.8	200.9	181.9
5	550.6	506.6	217.1	222.5	201.7
6	750.3	718.9	296.0	323.9	276.3
7	920.9	873.0	470.8	497.4	460.0
8	979.5	942.6	536.4	549.1	510.8
	g tensors of the ground Kramers doublet				
g_X	0.038	0.269	0.185	0.081	0.331
g_Y	0.088	0.841	0.401	0.142	0.973
g_Z	19.279	18.934	17.435	17.590	16.946
	angle of g_Z axis with the shortest Ln –N chemical bond (deg.)				
	8.48	11.35	84.67	85.99	87.22

The obtained ab initio results for individual metal sites were further used for the computation of the exchange spectrum and magnetic properties of the binuclear complexes using the POLY_ANISO program.[29, 37] The exchange interaction between Ln sites is considered within the Lines model[38] (see ESI for more details), while the contribution of the intramolecular dipole-dipole magnetic coupling is accounted exactly, since all the necessary data is available from the ab initio calculations. Best fitting Lines parameters of the exchange interaction for the investigated compounds are given in Table 3. On the basis of the resulting exchange spectrum of the entire system, all macroscopic magnetic properties were computed.

The magnetic interaction (exchange + dipolar) between the lowest Kramers doublets on sites can be cast in a good approximation by the non-collinear Ising Hamiltonian:

$$\hat{H}_{exch} = -J\hat{\tilde{s}}_{z1}\hat{\tilde{s}}_{z2} \qquad (1),$$

where $J = J_{dipolar} + J_{exchange}$ is the parameter of total magnetic interaction between metal sites and $\hat{\tilde{s}}_{zi} = 1/2$ is the pseudospin of the ground doublet state of the corresponding Dy and Er sites.

Table 3. Exchange and dipolar interactions (entering Eq.1) and the corresponding low-lying exchange spectrum of the Dy$_2$-biph and Dy$_2$-biph-crown$_2$ (cm^{-1}).

interaction	Dy$_2$-biph	Dy$_2$-biph-crown$_2$
dipolar*	-2.482	-2.504
exchange	1.056	7.253
	low-lying exchange spectrum of the binuclear compounds	
	0.000000	0.000000
	0.000021	0.021005
	0.767187	1.996495
	0.767212	2.024025
	90.716751	49.607745
	90.717581	49.648058
	90.819442	50.385569
	90.822345	50.412137
	90.928407	53.342034
	90.931136	53.371755
	91.044514	54.086462
	91.045231	54.099730
	…	…
	g$_z$ values in the two low lying exchange doublets states**	
	15.531	33.107
	35.315	18.411

* Only the term ($\sim z_1 z_2$) of the dipolar interaction is shown here. All terms were included in the POLY_ANISO calculation.

**g$_{X,Y}$ = 0 for non-Kramers doublets, in view of the Griffith theorem.[39]

From Table 3, we noticed that the dipolar coupling in **Dy$_2$-biph** and **Dy$_2$-biph-crown$_2$** is antiferromagnetic and of rather similar strength, while the exchange coupling is ferromagnetic and much stronger in the latter compound.

While in **Dy$_2$-biph** the exchange interaction is weaker than the dipolar one, in **Dy$_2$-biph-crown$_2$** the situation is opposite. The reason for sharp discrepancy in the exchange coupling of **Dy$_2$-biph** compared to **Dy$_2$-biph-crown$_2$** could be the presence of the two K$^+$ ions in the former compound that attract a significant amount of electronic density from the C$_8$ ring, promoting the interaction between lanthanide sites. While inner vs. outer-sphere differences have been previously observed for exchange coupling,[40] a switch of anti-ferromagnetic to ferromagnetic coupling has not been previously reported. The magnetism computed using the parameters reported in Table 3 compares relatively well with measured values (Figures 6, S8, and S9).

The insight offered by ab initio calculations allows for the rationalization of SMM behavior of the investigated compounds. Thus, the only compound showing peaks in the out-of-phase *ac* susceptibility in the absence of applied static magnetic field is **Dy$_2$-biph** (Figure S14), which has the highest on-site magnetic axiality (Table 2). For **Dy$_2$-biph-crown$_2$**, only weak peaks are observed in the presence of a static applied magnetic field, suppressing the QTM, which is in line with much larger values of g$_{X,Y}$ in the ground Kramers doublet of individual Dy ions. This is also true for both Er complexes, which also show large values of g$_{X,Y}$ in the ground doublet states (Table 2).

a)
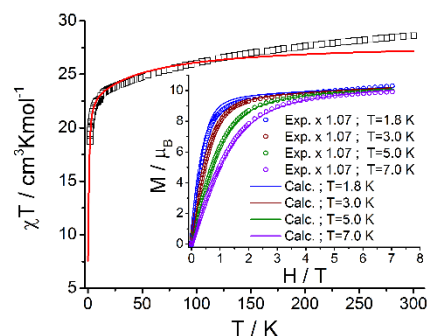
b)
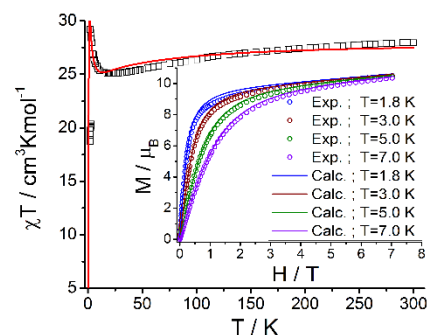
Figure 6. Comparison between measured (empty figures) and ab initio calculated (lines) magnetic susceptibility and molar magnetization (insets) for **Dy$_2$-biph** (a) and **Dy$_2$-biph-crown$_2$** (b).

CONCLUSIONS

We synthesized a series of inverse sandwich dysprosium, erbium, and gadolinium biphenyl complexes with and

8

without potassium coordinated to the neighboring phenyl ring by manipulating the molecules bound to potassium. The nature of the magnetic coupling between the lanthanide ions was surprisingly different: a ferromagnetic interaction was observed in **Dy$_2$-biph-crown$_2$**, **Er$_2$-biph**, and **Er$_2$-biph-crown$_2$**, each having lanthanide-lanthanide distances shorter than **Gd$_2$-biph**, **Gd$_2$-biph-crown$_2$**, and **Dy$_2$-biph**, for which antiferromagnetic coupling was observed. SMM behavior was observed in **Dy$_2$-biph** under zero dc field with an energy barrier of 34 K. This barrier significantly increased to 53 K with the application of a 900 Oe dc field, which suppressed QTM. For **Dy$_2$-biph**, the relaxation barrier primarily arises from the single-ion anisotropy of the dysprosium(III) ion. However, when dysprosium(III) and erbium(III) ions are coupled ferromagnetically, the observed barriers are reduced due to significant QTM since ferromagnetic coupling of the two half-integer spin leads to an integer ground state spin molecule. Nonetheless, it was remarkable to observe that the secondary coordination environment affects drastically the nature of the magnetic interaction in the two dysprosium systems and, subsequently, the magnet-like behavior shown by the slow relaxation of the magnetization.

ASSOCIATED CONTENT

Supporting Information. X-ray crystallography data, magnetic data, and ab initio calculation data. This material is available free of charge via the Internet at http://pubs.acs.org.

AUTHOR INFORMATION

Corresponding Author

pld@chem.ucla.edu
m.murugesu@uottawa.ca
liviu.ungur@chem.kuleuven.be

Present Addresses

[I] Current Address: Department of Chemistry, Massachusetts Institute of Technology, Cambridge, Massachusetts 02139, USA

Author Contributions

[&] These authors contributed equally.

### Notes
The authors declare no competing financial interest.

REFERENCES

1. Rinehart, J. D.; Long, J. R., *Chem. Sci.* **2011,** *2* (11), 2078-2085.
2. Woodruff, D. N.; Winpenny, R. E. P.; Layfield, R. A., *Chem. Rev.* **2013,** *113* (7), 5110-5148.
3. Layfield, R. A., *Organometallics* **2014,** *33* (5), 1084–1099.
4. Sorace, L.; Benelli, C.; Gatteschi, D., *Chem. Soc. Rev.* **2011,** *40* (6), 3092-3104.
5. Chilton, N. F.; Collison, D.; McInnes, E. J. L.; Winpenny, R. E. P.; Soncini, A., *Nat. Commun.* **2013,** *4*, 2551.
6. Rinehart, J. D.; Fang, M.; Evans, W. J.; Long, J. R., *J. Am. Chem. Soc.* **2011,** *133* (36), 14236-14239.
7. Rinehart, J. D.; Fang, M.; Evans, W. J.; Long, J. R., *Nat. Chem.* **2011,** *3* (7), 538-542.
8. Mills, D. P.; Moro, F.; McMaster, J.; van Slageren, J.; Lewis, W.; Blake, A. J.; Liddle, S. T., *Nat. Chem.* **2011,** *3* (6), 454-460.
9. Huang, W.; Dulong, F.; Wu, T.; Khan, S. I.; Miller, J. T.; Cantat, T.; Diaconescu, P. L., *Nat. Commun.* **2013,** *4*, 1448.
10. Diaconescu, P. L.; Arnold, P. L.; Baker, T. A.; Mindiola, D. J.; Cummins, C. C., *J. Am. Chem. Soc.* **2000,** *122* (25), 6108-6109.
11. Evans, W. J.; Kozimor, S. A.; Ziller, J. W.; Kaltsoyannis, N., *J. Am. Chem. Soc.* **2004,** *126* (44), 14533-14547.
12. Monreal, M. J.; Khan, S. I.; Kiplinger, J. L.; Diaconescu, P. L., *Chem. Commun.* **2011,** *47* (32), 9119-9121.
13. Patel, D.; Moro, F.; McMaster, J.; Lewis, W.; Blake, A. J.; Liddle, S. T., *Angew. Chem. Int. Ed.* **2011,** *50* (44), 10388-10392.
14. Arnold, P. L.; Mansell, S. M.; Maron, L.; McKay, D., *Nature Chem.* **2012,** *4* (8), 668-674.
15. Diaconescu, P. L.; Cummins, C. C., *Inorg. Chem.* **2012,** *51* (5), 2902-2916.
16. Vlaisavljevich, B.; Diaconescu, P. L.; Lukens, W. L.; Gagliardi, L.; Cummins, C. C., *Organometallics* **2013,** *32* (5), 1341-1352.
17. Patel, D.; Tuna, F.; McInnes, E. J. L.; McMaster, J.; Lewis, W.; Blake, A. J.; Liddle, S. T., *Dalton Trans.* **2013,** *42* (15), 5224-5227.
18. Camp, C.; Mougel, V.; Pécaut, J.; Maron, L.; Mazzanti, M., *Chem. Eur. J.* **2013,** *19* (51), 17528-17540.
19. Pangborn, A. B.; Giardello, M. A.; Grubbs, R. H.; Rosen, R. K.; Timmers, F. J., *Organometallics* **1996,** *15* (5), 1518-1520.
20. Bailey, P. J.; Coxall, R. A.; Dick, C. M.; Fabre, S.; Henderson, L. C.; Herber, C.; Liddle, S. T.; Lorono-Gonzalez, D.; Parkin, A.; Parsons, S., *Chem. Eur. J.* **2003,** *9* (19), 4820-4828.
21. Monreal, M. J.; Carver, C. T.; Diaconescu, P. L., *Inorg. Chem.* **2007,** *46* (18), 7226-7228.
22. Huang, W.; Upton, B. M.; Khan, S. I.; Diaconescu, P. L., *Organometallics* **2013,** *32* (5), 1379-1386.
23. Meyer, G.; Garcia, E.; Corbett, J. D., The Ammonium Chloride Route to Anhydrous Rare Earth Chlorides—The Example of YCl_3. In *Inorganic Syntheses*, John Wiley & Sons, Inc.: 2007; pp 146-150.
24. Le Roy, J. J.; Jeletic, M.; Gorelsky, S. I.; Korobkov, I.; Ungur, L.; Chibotaru, L. F.; Murugesu, M., *J. Am. Chem. Soc.* **2013,** *135* (9), 3502-3510.
25. Shannon, R., *Acta Cryst. A* **1976,** *32* (5), 751-767; see also http://abulafia.mt.ic.ac.uk/shannon/.
26. Cucinotta, G.; Perfetti, M.; Luzon, J.; Etienne, M.; Car, P.-E.; Caneschi, A.; Calvez, G.; Bernot, K.; Sessoli, R., *Angew. Chem. Int. Ed.* **2012,** *51* (7), 1606-1610.
27. Ishikawa, N.; Iino, T.; Kaizu, Y., *J. Am. Chem. Soc.* **2002,** *124* (38), 11440-11447.
28. Aquilante, F.; Vico, L. D.; Ferre, N.; Ghigo, G.; Malmqvist, P. A.; Neogrady, P.; Pedersen, T. B.; Pitonak, M.; Reiher, M.; Roos, B. O.; Serrano-Andres, L.; Urban, M.; Veryazov, V.; Lindh, R., *J. Comput. Chem.* **2010,** *31*, 224-247.
29. Chibotaru, L. F.; Ungur, L. J., *Chem. Phys.* **2012,** *137*, 064112.
30. Ungur, L.; Roy, J. J. L.; Korobkov, I.; Murugesu, M.; Chibotaru, L. F., *Angew. Chem. Int. Ed.* **2014,** *53*, 4413-4417.
31. Ungur, L.; Chibotaru, L. F., *Phys. Chem. Chem. Phys.* **2011,** *13*, 20086-20090.
32. Chibotaru, L. F.; Ungur, L.; Aronica, C.; Elmoll, H.; Pilet, G.; Luneau, D., *J. Am. Chem. Soc.* **2008,** *130*, 12445-12455.
33. Ungur, L.; Heuvel, W. V. d.; Chibotaru, L. F., *New J. Chem.* **2009,** *33*, 1224-1230.
34. Marx, R.; Moro, F.; Dörfel, M.; Ungur, L.; Waters, M.; Jiang, S. D.; Orlita, M.; Taylor, J.; Frey, W.; Chibotaru, L. F.; Slageren, J. v., *Chem. Sci.* **2014,** *5*, 3287-3293.
35. Roos, B. O.; Veryazov, V.; Widmark, P.-O., *Theor. Chem. Acc.* **2004,** *111*, 345.
36. Abragam, A.; Bleaney, B., *EPR of Transition Ions*. Oxford University Press: Oxford, 1970; Table 20.
37. Ungur, L.; Thewissen, M.; Costes, J.-P.; Wernsdorfer, W.; Chibotaru, L. F., *Inorg. Chem.* **2013,** *52*, 6328-6337.
38. Lines, M. E., *J. Chem. Phys.* **1971,** *55*, 2977-2984.
39. Griffith, J. S., *Phys. Rev.* **1963,** *132*, 316-319.
40. Meihaus, K. R.; Corbey, J. F.; Fang, M.; Ziller, J. W.; Long, J. R.; Evans, W. J., *Inorg. Chem.* **2014,** *53*, 3099-3107.
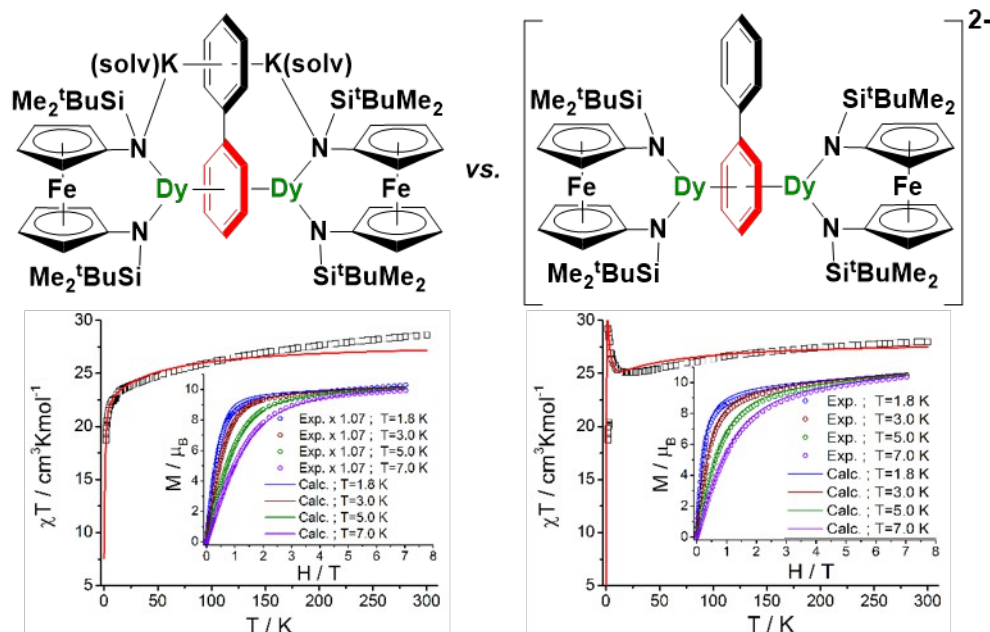
Inverse sandwich biphenyl complexes, $[(NNTBS)Ln]_2(\mu\text{-biphenyl})[K(\text{solvent})]_2$ (NN^{TBS} = 1,1'-fc(NSi^{t}BuMe$_2$)$_2$; Ln = Gd, Dy, Er; solvent = Et$_2$O, toluene; 18-crown-6), containing a quadruply reduced biphenyl ligand, were synthesized and their magnetic properties measured. One of the dysprosium biphenyl complexes exhibits antiferromagnetic coupling and single-molecule magnet behavior with U_{eff} of 34 K under zero applied field. The solvent coordinated to potassium affected drastically the nature of the magnetic interaction, with the other dysprosium complex showing ferromagnetic coupling.